# Controlling the double layer of platinum by selective passivation of step sites using adatom modification

Fröhlich, N.L.; Hu, Y.; Larsson, A.L.; Koper, M.T.M.

JACS
JOURNAL OF THE AMERICAN CHEMICAL SOCIETY
pubs.acs.org/JACS



Article

# Controlling the Double Layer of Platinum by Selective Passivation of Step Sites Using Adatom Modification

Nicci L. Fröhlich, Yifan Hu, Alfred Larsson, and Marc T. M. Koper*

Cite This: J. Am. Chem. Soc. 2026, 148, 31171−31180

Read Online

ACCESS | Metrics & More | Article Recommendations | Supporting Information

**ABSTRACT:** The structure of the electric double layer at platinum electrodes remains incompletely understood, even for the model Pt(111)/$HClO_4$ interface, which deviates significantly from Gouy−Chapman−Stern theory. While Pt(111) exhibits a true double-layer window (0.40−0.60 $V_{RHE}$) that enables direct measurement of the double-layer capacitance, stepped Pt surfaces do not because hydrogen and/or hydroxyl species adsorb at low-coordinated step sites across the entire potential range. We previously showed that hydroxyl adsorption on (110)-steps is potential-independent within this nominal double-layer window, leading to decreasing capacitance with increasing (110)-step density due to suppression of the step Helmholtz capacitance. In contrast, (100)-steps exhibit potential-dependent hydroxyl adsorption that introduces a substantial pseudocapacitive contribution and increases capacitance with step density. Here, we selectively passivate Pt step sites by depositing Au* and Ag* adatoms. We find that $Au^*_{step}$-modification suppresses step-specific adsorption, restoring predominantly electrostatic behavior for (100)-type stepped Pt surfaces and reversing the capacitance trends observed for the bare stepped surfaces. In contrast, $Ag^*_{step}$-modification introduced an additional chemical contribution, manifested as substantially increased capacitance and enhanced CO oxidation activity due to adsorption of oxophilic species on Ag*. These results demonstrate that Pt step-site chemistry, and consequently the electrical double-layer structure and electrocatalytic activities, can be tuned and probed to a remarkable degree of controllability through selective adatom modification.

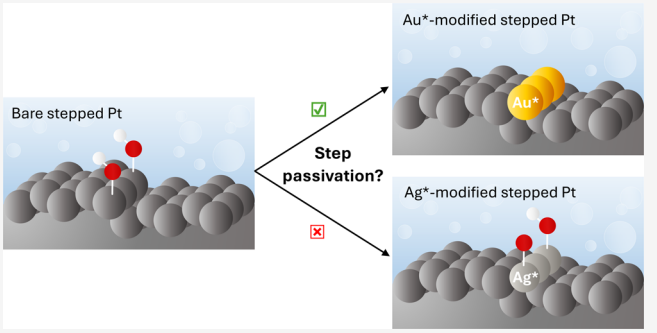


## INTRODUCTION

Elucidating the structure of the electrical double layer is imperative for understanding the factors governing electrocatalytic activity. Despite extensive study, however, the electrochemistry of platinum remains incompletely understood. Even the most key, model electrochemical interface, Pt(111)/$HClO_4$, deviates significantly from widely established Gouy−Chapman−Stern (GCS) description of the electric double layer.[1] This interface is particularly important for the fundamental understanding of Pt electrodes because Pt(111) exhibits a true double layer window, i.e., an adsorbate-free potential region between 0.40−0.60 $V_{RHE}$, bounded by hydrogen (0.05−0.40 $V_{RHE}$) and hydroxyl (0.60−0.85 $V_{RHE}$) adsorption regions.[2−4] Within this window, the measured capacitance arises from purely electrostatic interactions, enabling direct determination of the double-layer capacitance. At low electrolyte concentrations (0.1 mM $HClO_4$), a capacitance minimum can be observed at the potential of zero free charge (0.54 $V_{RHE}$ at pH 4; 0.30 $V_{SHE}$), where the diffuse-layer (Gouy−Chapman) capacitance dominates.[5,6] Notably, this measured capacitance substantially exceeds that predicted by GCS theory and has been attributed to an increased near-surface ion concentration arising from electrostatic rather than chemical effects.[7−9]

Although the Pt(111)/$HClO_4$ interface is important from a model point-of-view, Pt(111) is not representative of industrially relevant poly- or nanocrystalline Pt electrodes, which contain a distribution of lower-coordinated sites such as steps, kinks, and/or defects.[10] These sites exhibit a higher affinity for water dissociation than Pt(111) meaning that all Pt surfaces, other than Pt(111), are covered by hydrogen and/or hydroxyl species across the entire potential range and therefore lack true double-layer windows.[2,11,12] While the influence of such low-coordinated sites on electrocatalytic activity has been widely studied, their impact on the structure of the electric double-layer has received considerably less attention despite its importance.[13−15]

In recent work,[16] we showed that introducing lower-coordinated step sites of (110)- and (100)-orientation onto a (111)-terrace (i.e., studying (110)-/(100)-stepped Pt single

Received: April 7, 2026
Revised: June 5, 2026
Accepted: June 8, 2026
Published: July 14, 2026







https://doi.org/10.1021/jacs.6c07209
J. Am. Chem. Soc. 2026, 148, 31171−31180

crystals) has a marked effect on the capacitance measured within the (111) double-layer window (0.40−0.60 $V_{RHE}$). Specifically, the capacitance decreases with increasing (110)-step density but increases with increasing (100)-step density, which we attributed to the presence of $OH_{ads}$ at the step sites within this potential window. The presence of such species is evidenced, in combination with other techniques,[12,17] by the blank voltammograms of these stepped surfaces, which display characteristic $H_{ads}/OH_{ads}$ exchange peaks in the hydrogen adsorption window (at 0.13 $V_{RHE}$ for (110)- and 0.30 $V_{RHE}$ for (100)-type steps, respectively).[18,19] These peaks indicate that as hydrogen gets de(ad-)sorbed, hydroxyl is simultaneously ad-(de)sorbed, implying that the (110)- and (100)-step sites retain a (partial) $OH_{ads}$ coverage within the (111) double-layer window. It followed that the step nature-dependent capacitance trends could be rationalized if the $OH_{ads}$ coverage on (110)-type steps is potential-independent within this potential region, whereas the $OH_{ads}$ coverage on (100)-type steps varies with potential. The latter introduces an additional adsorption capacitance that increases the total measured capacitance, which was also found to hold true for much more structurally heterogeneous polycrystalline Pt electrodes.[10] The potential-dependent $OH_{ads}$ coverage on (100)-step sites in this potential window was also supported by Parsons−Zobel (PZ) analysis, which shows a decreasing slope with increasing (100)-step density, consistent with an adsorption capacitance occurring in parallel with the double-layer capacitance charging. In contrast, the slope remains unchanged with increasing (110)-step density.[16] The decreased capacitance observed upon introducing (110)-steps was instead attributed to suppression of the Helmholtz capacitance of the step due to the presence of $OH_{ads}$. These findings highlight the marked influence of step-site chemistry on the electric double layer structure and demonstrate that adsorption processes can significantly convolute the measured capacitance response.

Motivated by these findings, we sought to selectively passivate step sites on stepped Pt single crystal electrodes by suppressing the $H_{ads}/OH_{ads}$ exchange intrinsic to the Pt step sites. Such passivation would reduce the structure sensitivity of the capacitance measured in the double-layer window related to adsorption events occurring on step sites and enable a controlled methodology to probe the electrode/electrolyte interface at a fundamental level by disentangling adsorption and structural contributions to the capacitance behavior. Previous studies have demonstrated that step decoration with foreign metal adatoms can successfully selectively tune electrocatalytic activity of stepped Pt electrodes, e.g., in the oxygen reduction and hydrogen evolution reactions.[20−23] However, similar to their bare counterparts, analogous investigations of their influence on electrical double-layer properties remain scarce. To this end, we study here the electric double-layer properties of heterobimetallic $M^*_{step}$/Pt($hkl$) surfaces (where M* denotes the metal adatom) in which a more chemically inert metal than Pt is deposited selectively at the step sites of both (110)- and (100)-stepped Pt single crystals. Au and Ag are of particular interest in this context as both metals are widely used as model electrodes in double-layer studies due to their chemical inertness,[24,25] suggesting that they could quench the intrinsic chemistry of Pt step sites without themselves introducing chemical effects. Moreover, previous work indicates that both metals preferentially deposit at step sites.[20,21,23]

Assuming predominantly selective step deposition and greater chemical inertness than Pt step atoms, step passivation should then manifest in a reversal of the step-nature dependent trends previously observed on the bare stepped Pt electrodes:[16] For (110)-stepped Pt surfaces, passivation should increase the capacitance in the double-layer window by removing the suppression of the step Helmholtz capacitance caused by $OH_{ads}$. In contrast, for (100)-stepped Pt electrodes the capacitance should decrease because quenching the potential-dependent $OH_{ads}$ would suppress the additional adsorption capacitance observed for the bare (100)-stepped Pt surfaces. We reveal here that these predicted trends (and implicitly true step passivation) are clearly observed for $Au^*_{step}$/Pt($hkl$) heterobimetallic surfaces, but not for $Ag^*_{step}$/Pt($hkl$) heterobimetallic surfaces. Instead, $Ag^*_{step}$/Pt($hkl$) heterobimetallic surfaces always displayed a large additional capacitance with increasing $Ag^*_{step}$ coverage, which we attribute to oxophilic species (i.e., OH/O species) adsorbed on Ag* as also evidenced by an enhanced activity for CO oxidation compared with the corresponding bare electrodes.[26−29] These results demonstrate that selective adatom modification on stepped Pt electrodes provides a methodology for disentangling adsorption and geometric contributions to the interfacial capacitance of stepped Pt electrodes by quenching the intrinsic chemistry occurring at Pt step sites.

## EXPERIMENTAL SECTION

### Electrochemical Measurement and Chemicals

The cleaning of glassware, cyclic voltammetry (CV) and Ohmic drop compensation procedures used in this work followed previously published protocols.[5,30] Electrochemical experiments were carried out using a VSP-300 potentiostat from Biologic. Disc-type single crystal Pt(111) (diameter 3 mm, MaTeck, 99.999%), Pt(S)-[($n$-1)(111)x-(110)] electrodes with $n$ = 14, 10, and 5 (diameter 4 mm, MaTeck, 99.999%) and Pt(S)-[$n$(111)x(100)] electrodes with $n$ = 29, 9, and 6 (diameter 4 mm, Surface Preparation Laboratory and Mateck, 99.999%, respectively) served as working electrodes. All potentials in this manuscript are reported versus the reversible hydrogen electrode (RHE) scale and were Ohmic drop-corrected where appropriate.

Electrode preparation followed the Clavilier flame-annealing method.[31,32] Briefly, the single crystals were annealed in two butane torches for 45s and subsequently cooled in a mixture of $H_2$/Ar (ratio 1:1, flow rate 200 mL $min^{-1}$ for each gas) for at least 4 min. After cooling, a droplet of ultrapure water (in the same cell as the crystal was cooled) was placed on the electrode surface, and the electrode was immediately transferred to the electrochemical cell. The cell was then purged with Ar for another 15 min prior to measurement.

Diluted $HClO_4$ (60% Merck Suprapur) electrolyte was prepurged with Ar gas (Linde 5.0, ≥99.999%) through polytetrafluoroethylene (PTFE) gas tubing to prevent $O_2$ permeation prior to electrochemical measurements. All double-layer capacitance measurements, as well as determining the relative adatom coverage in the step (see adatom deposition Methods section) were carried out in 0.1 mM $HClO_4$ electrolyte.

$NaClO_4 \cdot H_2O$ (≥99% Merck EMSURE) and KMSA (>99% Thermo Scientific) were used for salt additions where specified. For the electrodeposition procedure, $HAuCl_4$ (99.995%, trace metals basis, Sigma-Aldrich) and $AgClO_4$ (99.999%, trace metals basis, Sigma-Aldrich) salts were used.

### Parsons−Zobel Plot Measurements

The blank electrolyte measurement was always made in 0.1 mM $HClO_4$ to which $x$ mM $NaClO_4$, or $x$ mM KMSA was added depending on the measurement. The inverse of the differential capacitance minimum in the double-layer window (i.e., at the





https://doi.org/10.1021/jacs.6c07209
J. Am. Chem. Soc. 2026, 148, 31171−31180

potential of zero free charge, $E_{pzfc}$) was plotted on the $y$-axis, measured using CV, $\nu$ = 5 mV $s^{-1}$. On the $x$-axis, the inverse of the Gouy−Chapman capacitance, $C_{GC}$, at the $E_{pzfc}$ at different bulk ion concentrations, $c$, is plotted as according to eq 1:[1]

$$C_{GC}(E_{pzfc}) = \left(\frac{2(zF)^2\varepsilon_s\varepsilon_0 c}{RT}\right)^{1/2} \quad (1)$$

where $z$ is the charge number of electrolyte ions, $F$ is Faraday's constant, $R$ is the gas constant, $\varepsilon_s$ is the solvent dielectric constant, $\varepsilon_0$ is the vacuum permittivity and $T$ is the temperature. The slope gives the deviation from Gouy−Chapman theory, whereas the inverse of the intercept on the $y$-axis gives the Helmholtz capacitance of the surface.

## Adatom Deposition and Relative Step Coverage Calculation

For adatom deposition, $10^{-6}$ M $HAuCl_4$, or $AgClO_4$ (depending on the metal to be deposited), were dissolved in 0.1 M $HClO_4$ in a dedicated electrochemical cell which was then purged with Ar prior to electrodeposition just as for the other electrochemical measurements. To deposit the metal, a freshly annealed single crystal was brought into a hanging meniscus configuration in the electrodeposition solution at 0.6 V and then cycled in the hydrogen adsorption region between 0.07−0.35 V at 50 mV $s^{-1}$ (where more cycles lead to higher coverages, typically around 10−100 cycles were required). If only a small adatom coverage was desired a constant potential of 0.1 V for ∼5 s was applied instead of employing CV cycling. The intensity of the step-related peak is directly correlated to the amount of metal deposited (see eq 2) allowing real time monitoring of the adatom step coverage. Once the desired coverage was achieved, a CA of 0.1 V was applied to avoid ensure no residual chloride adsorbates from the deposition solution remained on the surface and the meniscus contact was broken. The adatom modified single crystal was then rinsed thoroughly with ultrapure water before being transferred to the electrochemical measurement cell. Note that very high coverages were more difficult to reach, especially in the case of Au* deposition, likely because of the overpotential deposition potentials being applied (i.e., Au* bulk agglomeration is also favorable at these potentials, not just selective deposition on Pt step sites).[33] For Ag*, the overpotential applied was less significant meaning predominantly selective deposition on the step sites is more readily achievable.[34] Therefore, only submonolayer step coverages for both Ag* and Au* were achievable (although a higher Ag* coverage was achieved due to the lower overpotential applied) and reported here.

To remove the adatoms from the Pt single crystal after electrochemical measurements, the crystal was etched in concentrated $HNO_3$ (65% Merck EMSURE) which consisted of first dipping the entire crystal in $HNO_3$, then lightly flame annealing the crystal (to temperatures before the crystal begins to glow red) and then dipping the crystal again into the concentrated $HNO_3$. This process was repeated 5 times, after which the crystal was flame annealed as normal, and the surface quality checked again using CV prior to further measurement.

The relative adatom coverage in the step, $\theta_{M*}^{step}$, was calculated as according to eq 2:[21]

$$\theta_{M*}^{step} = \frac{Q_H^{S,0} - Q_H^{S,M*}}{Q_H^{S,0}} \quad (2)$$

where $Q_H^{S,0}$ is the charge under the step-related peak in the hydrogen adsorption region for the bare surface and $Q_H^{S,M*}$ the charge under the step-related peak in the hydrogen adsorption region for the adatom modified surface (see SI Figure 1a for an example of the designation of $Q_H^{S,0}$ and $Q_H^{S,M*}$, respectively).

## CO Oxidation Measurements

Prior to CO oxidation measurements, the surface quality and adatom coverage were checked as normal in Ar-purged 0.1 mM $HClO_4$ electrolyte. The meniscus contact was then broken and the electrolyte purged (both through the electrolyte and overhead) with CO gas (Linde 4.7, ≥ 99.997%) for 15 min. The CO flow through the electrolyte was then turned off (but the CO flow overhead was maintained) and the electrode was brought back into hanging meniscus configuration at 0.1 V and the current allowed to stabilize for 30 s. After Ohmic-drop correction, the CO oxidation activity was then measured in 0.1 mM $HClO_4$ electrolyte using a linear sweep voltammogram using a scan rate of 10 mV $s^{-1}$ where the upper vertex potential was set to 0.9 V. Note here that 0.1 mM $HClO_4$ was chosen as opposed to the more conventional 0.1 M $HClO_4$ electrolyte to keep the electrolyte parameters the same as those used for the capacitance measurements. More specifically, if (as hypothesized in the main manuscript) hydroxyl adsorbates are present on Ag*, then it is well-known that this adsorption is pH-dependent[35] meaning that keeping the pH constant for the CO oxidation measurements was important for a direct comparison between the presence of such oxophilic species on the Ag* adatoms and the capacitance results.

## X-ray Photoelectron Spectroscopy (XPS) Measurements

XPS spectra were measured *ex situ* in vacuum using a Scientia lab-based system equipped with a monochromatic Al K$\alpha$ X-ray source described in ref.[36] XPS was measured after taking out the sample under potential control, rinsing with ultrapure water, and drying with compressed air. The sample was then immediately transferred into the XPS chamber. The Ag 3d and Pt $4d_{5/2}$ core levels were measured and chosen due to their proximity in binding energy. This ensures a similar probing depth and, therefore, a straightforward comparison of intensity ratios. All spectra are background-subtracted using a Shirley background.

To quantify the Ag* coverage on the steps, the Ag overlayer thickness, $d$, was first calculated from the XPS intensities as shown eq 3:[37]

$$d = \lambda^{Ag}\cdot\ln\left(1 + \frac{N^{Pt}\lambda^{Pt}I^{Ag}}{N^{Ag}\lambda^{Ag}I^{Pt}}\right) \quad (3)$$

where $\lambda^{Ag}$ and $\lambda^{Pt}$ are the inelastic mean free paths of the photoelectrons in Ag and Pt, respectively; $N^{Ag}$ and $N^{Pt}$ are the atomic densities of Ag and Pt, respectively; and $I^{Ag}$ and $I^{Pt}$ are the intensities of the Ag and Pt core levels, respectively. The inelastic mean free path was calculated using the QUASES-IMFP-TPP2M Ver. 3.0 software using electron energies of 1137 eV. The atomic densities were calculated as the ratio between the density and molar mass. The intensities were corrected for the cross section taken from refs.[38,39] For Pt, the intensity was multiplied by (1 + 3/5) to account for the fact that only the Pt $4d_{5/2}$ core level was measured. The ratio 3/5 originates from the intensity ratio between the $d_{5/2}$:$d_{3/2}$ of 3:2. When using intensity ratios to calculate thicknesses based on XPS data, the intensities related to the whole core level (e.g., Pt $4d_{5/2}$ and $4d_{3/2}$) must be used. All the parameters used for the calculations are shown in Table 1. Once the overlayer thickness was obtained, it was converted into monolayer coverage by dividing by the size of the Ag atom (2.9 Å). To then obtain the Ag* coverage along the step edges, the coverage was divided by the coverage of steps on the surface (i.e., 0.11 ML in the case of Pt(554)).

**Table 1. Parameters Used for XPS Overlayer Calculation**

| Parameter | Ag | Pt |
|---|---|---|
| Inelastic mean free path (Å) | 16.23 | 13.09 |
| Cross section (Mbarn) | 0.2474 | 0.2642 |
| Atomic density (mol $cm^{-3}$) | 0.11 | 0.097 |

# RESULTS AND DISCUSSION

Figure 1 shows the blank cyclic voltammograms (CVs) of Pt(554) and Pt(544) taken in 0.1 mM $HClO_4$. We focus our study here on these two single crystals as both electrodes consist of (111)-terrace sites of similar width (ca. 10 atoms wide) which are separated by monatomic step sites which are





https://doi.org/10.1021/jacs.6c07209
J. Am. Chem. Soc. 2026, 148, 31171−31180

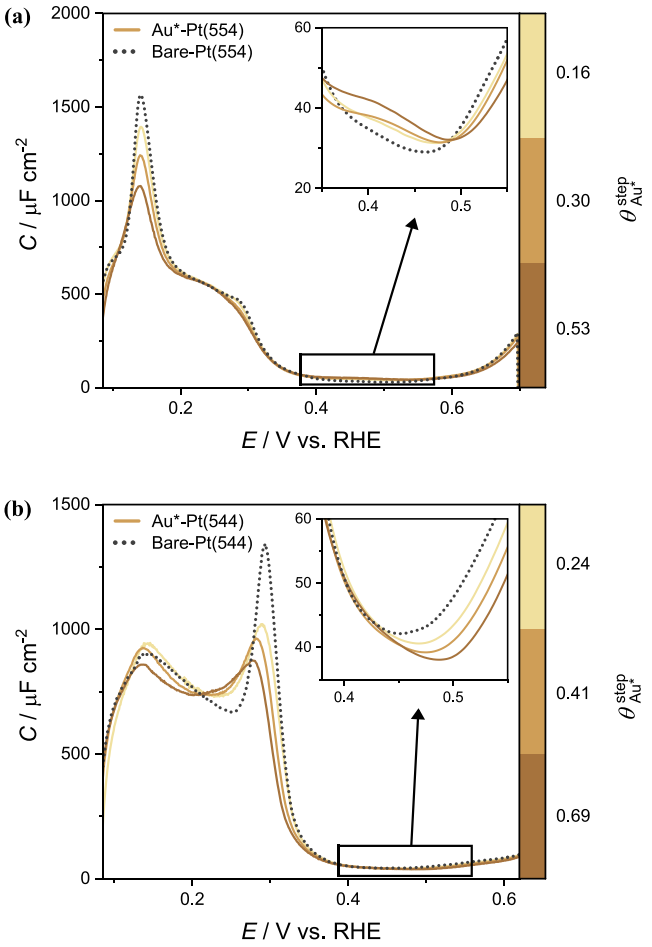


**Figure 1.** Capacitance curves for (a) Au*$_{step}$-Pt(554) ($\theta^{step}_{Au*}$ = 0.16–0.53), (b) Au*$_{step}$-Pt(544) ($\theta^{step}_{Au*}$ = 0.24–0.69), measured in 0.1 mM $HClO_4$ using CV, $\nu$ = 5 mV $s^{-1}$. Coverage on the step ($\theta^{step}_{Au*}$) was calculated as according to eq 2 in the Experimental Section. Corresponding CVs of the respective bare surfaces are also shown (dashed lines). Insets show zoom in of capacitance in the double-layer window.

predominantly (110)- in nature in the case of Pt(554), and predominantly (100)- in the case of Pt(544), i.e., we can directly compare the effect of adatom modification on two different step types. The close agreement of the CVs shown in Figure 1 with previously reported voltammetric fingerprints for these vicinal surfaces indicate a high degree of surface order and suggests that defect densities (e.g., kink sites) are relatively low.[40,41] Furthermore, for these stepped surfaces, we can exclude step bunching instabilities, which would potentially complicate analysis.[41]

In the blank CVs of Pt(554) and Pt(544), large pseudocapacitive peaks can be observed at 0.13 V (Figure 1a) and 0.30 V (Figure 1b), respectively, which have been attributed to $H_{ads}/OH_{ads}$ exchange on monatomic (110)- and (100)-step sites, respectively (i.e., as soon as hydrogen is ad-(de)sorbed from the step, a hydroxyl species is concurrently de(ad-)sorbed).[11,18,19] Unlike for Pt(111), where the adsorption of $H_{ads}$ and $OH_{ads}$ species are well-separated by a 200 mV wide double-layer window between 0.40–0.60 V, $H_{ads}/OH_{ads}$ exchange occurs as a simultaneous process on step sites (both (110)- and (100)-type steps) because of their increased affinity for water dissociation compared to (111)-sites. Therefore, within the Pt(111) double-layer window (0.40–0.60 V), stepped Pt single crystal surfaces will always have some $OH_{ads}$ coverage in the step sites. In accordance with our recent findings,[16] Pt(554) has a lower capacitance in the double-layer window than Pt(111), but Pt(544) has a larger capacitance (see insets in Figure 1a and b, respectively). As discussed in the Introduction, this step nature-dependent capacitance behavior was attributed to a potential-independent $OH_{ads}$ coverage on (110)-steps (in the case of Pt(554)), but a potential-dependent $OH_{ads}$ coverage on (100)-steps (in the case of Pt(544)). In the former case, the decreasing capacitance with increasing (110)-step density can be attributed to a very low step Helmholtz capacity, $C_H$, due to the presence of $OH_{ads}$ on (110)-steps, whereas in the latter case, the potential-dependent $OH_{ads}$ coverage leads to an additional adsorption capacitance contribution which dominates and therefore an overall increase in the capacitance is observed.

In order to reverse these step-dependent trends, i.e., make the steps inactive and block the chemistry occurring there (specifically the $H_{ads}/OH_{ads}$ exchange), we electrodeposit Au predominantly selectively in the step sites (denoted as Au* in its adatom form here) which is a chemically inert metal typically used for double-layer studies.[25] As can be observed from Figure 1a, the only observed effect on the voltammetry of Pt(554) after deposition of Au* is a quenching of the (110)-step related peak (at 0.13 V) resulting from a successful selective blocking of the $H_{ads}/OH_{ads}$ exchange process on the (110)-step sites. The hydrogen adsorption on the (111)-terrace remains unaffected by this adatom modification with respect to the blank CV of the corresponding bare surface. Therefore, Au* deposition is seemingly highly selective for the (110)-step sites of Pt(554) over that of the (111)-terrace sites. A similar step selectivity of the Au* can be observed for the (100)-step sites of Pt(544) (Figure 1b). However, in contrast to Pt(554), a small negative shift of the (100)-step-related $H_{ads}/OH_{ads}$ exchange peak is observed with increasing Au* coverage. The origin of this shift is unclear, but it may reflect a modification of the adsorption energetics of neighboring Pt step atoms induced by Au* at the step edge. Interestingly, this effect is not observed for the (110)-step sites of Pt(554), suggesting a possible dependence on the local step geometry. However, since this behavior does not affect the main conclusions of this work, a more detailed interpretation is beyond the scope of the present study.

Moreover, the predominantly selective deposition of Au* on the step sites was previously elucidated using X-ray photoelectron spectroscopy (XPS) on both (110)- and (100)-stepped Pt surfaces,[20] as well as under ultrahigh vacuum (UHV) conditions using scanning tunnelling microscopy (STM) for Pt(111).[42] This step site selectivity was attributed to a smaller surface energy of Au atoms compared to Pt using first-principles calculations.[43–45] This lower surface energy of the Au has the consequence that the less stable, lower-coordinated Pt step sites were found to be more favorable for adsorption compared to (111)-sites, in accordance with the CV results presented here (Figure 1). It should be noted that in the case of Pt(544), a broad peak centered at ca. 0.13 V in the blank CV can be observed (Figure 1b) superimposed on the hydrogen adsorption charge of Pt(111). This peak results from common (110)-step defects present on the (100)-stepped single crystal Pt surface which behave in a similar way to monatomic (110)-steps.[20,46,47] In accordance with the preferential adsorption of Au* on lower-coordinated sites, Au*$_{step}$-modification also leads to a small quenching of this





https://doi.org/10.1021/jacs.6c07209
J. Am. Chem. Soc. 2026, 148, 31171–31180

(110)-defect peak in the case of Pt(544) but, importantly, does not affect hydrogen adsorption on the (111)-terrace as also observed for Pt(554). Nonetheless, the proportion of these (110)-defect sites is smaller than the (100)-step sites for this crystal, meaning that the changes in the total capacitance response are still dominated by changes to the adsorption on (100)-step sites. Regardless, it can be concluded that Au*-modification is highly selective for the (110)- and (100)-step sites, and thus all capacitance behavior for the Au*$_{step}$/Pt($hkl$) heterobimetallic surfaces is likely attributable to selective blocking of the chemistry intrinsic to the Pt step sites themselves (i.e., the $H_{ads}/OH_{ads}$ exchange process occurring there), rather than due to a significant deposition on (111)-terrace sites.

Bearing this selective deposition in mind, discrepant behavior in the capacitance in the double-layer window can be observed upon Au*$_{step}$-modification between Pt(554) and Pt(544) (see insets Figure 1). Increasing Au*$_{step}$-coverage ($\theta^{step}_{Au*}$) leads to an increased capacitance in the double-layer window for Pt(554) (Figure 1a), but a decreased capacitance for Pt(544) (Figure 1b). Importantly, in both cases the double-layer capacitance tends toward that of Pt(111),[5,16] i.e., capacitance in the double-layer window of bare Pt(554) < Au*$_{step}$-modified Pt(554) < Pt(111) < Au*$_{step}$-modified Pt(544) < bare Pt(544). These results strongly suggest that Au* does indeed passivate the step sites predominantly selectively as the step-dependent trends observed for bare stepped Pt electrodes become reversed upon Au*$_{step}$-modification likely due to blocking of the $H_{ads}/OH_{ads}$ exchange occurring at the steps. The blocking of this exchange process manifests itself in an increasing capacitance upon increasing $\theta^{step}_{Au*}$ in the case of Pt(554) as the suppression of the step $C_H$ due to $OH_{ads}$ becomes quenched, whereas for Pt(544), an increasing $\theta^{step}_{Au*}$ simply blocks the adsorption capacitance associated with (100)-sites and therefore leads to a decreased capacitance.

This true step passivation and the blocking of the pseudocapacitive processes occurring on bare (100)-step sites upon Au*$_{step}$-modification can be further visualized using a Parsons-Zobel (PZ) plot analysis. Ideally, the slope of the PZ plot should tend toward unity, however, it is now well-established that Pt(111) has a significantly suppressed slope (ca. 0.04, Figure 2), which has been previously attributed to a higher near-surface ion concentration than predicted by GCS theory.[6−9] As discussed in a previous publication and reproduced here,[16] the PZ plot slope of bare Pt(544) is significantly lower than the PZ plot slope of Pt(111) (Figure 2a), whereas Pt(554) has the same PZ plot slope as for Pt(111) (Figure 2b). These discrepant trends can again be explained by the fact that (100)-steps are pseudocapacitive in nature in the double-layer window (between 0.40 − 0.60 V) owing to a potential-dependent $OH_{ads}$ coverage, where this is not observed for (110)-stepped Pt surfaces. As described in detail in ref,[16] this pseudocapacitive process occurs in parallel with the double-layer (or free charge) capacitance terms and leads to the suppressed PZ plot slopes observed for (100)-stepped Pt surfaces, but not for (110)-stepped Pt surfaces where no such process occurs. Instead, the only difference observable in the PZ plot for (110)-stepped Pt surfaces compared to Pt(111) is that (110)-type steps lead to a decrease in the $C_H$ (approximated from the inverse of the $y$-intercept as this corresponds to an infinite bulk ion concentration, Figure 2a), which is in accordance with the

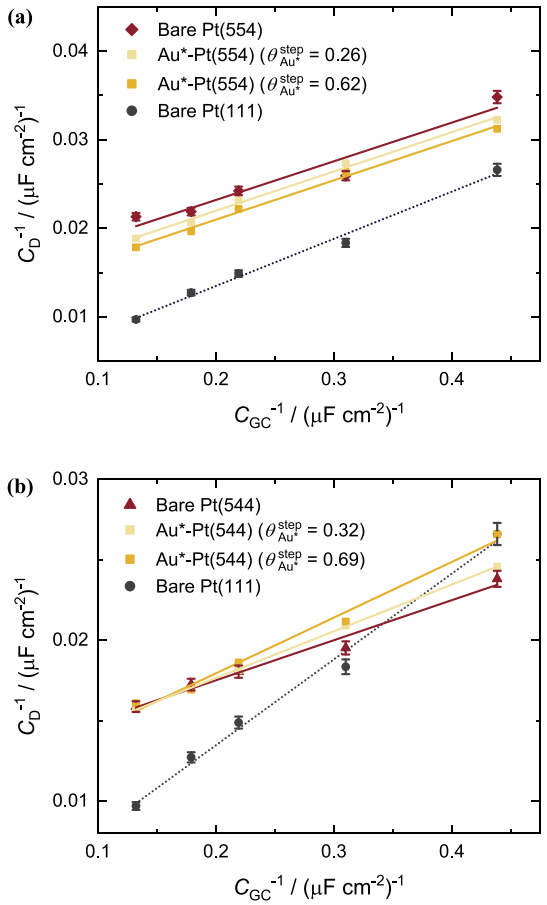


**Figure 2.** Parsons−Zobel plots of (a) bare Pt(554) (brown diamonds), Au*$_{step}$-Pt(554) ($\theta^{step}_{Au*}$ = 0.26, 0.62) (light and dark gold squares, respectively), bare Pt(111) (black circles) and (b) bare Pt(544) (brown triangles), Au*$_{step}$-Pt(544) ($\theta^{step}_{Au*}$ = 0.32, 0.69) (light and dark gold squares, respectively), bare Pt(111) (black circles) measured in 0.1 mM $HClO_4$ + $x$ mM $NaClO_4$ using CV, $\nu$ = 5 mV s$^{-1}$. Data for the bare surfaces are presented as mean values ± standard deviation of 3 data sets represented as error bars. Error bars are not included for the Au*$_{step}$-modified electrodes because independently prepared adatom-modified surfaces exhibit small unavoidable variations in coverage and therefore replicate measurements primarily reflect coverage variability rather than intrinsic capacitance uncertainty.

low $C_H$ of the steps caused by the presence of (a potential-independent coverage of) $OH_{ads}$.

Importantly, upon Au*$_{step}$-modification, these step nature dependent trends on the bare stepped Pt surfaces become reversed. In the case of Pt(554) (Figure 2a), Au*$_{step}$-modification does not affect the PZ plot slope, remaining the same as that of both Pt(111) and bare Pt(554) irrespective of $\theta^{step}_{Au*}$. However, when modifying Pt(554) with Au* and effectively removing the $OH_{ads}$ at the step sites, the $C_H$ of the Au*$_{step}$-Pt(554) surface increases slightly with increasing $\theta^{step}_{Au*}$ relative to that of the bare Pt(554), tending toward the value of Pt(111) indicating that indeed less $OH_{ads}$ is present on the (110)-step sites after modification. In the case of Pt(544) (Figure 2b), Au*$_{step}$-modification leads to an increasing PZ plot slope with increasing $\theta^{step}_{Au*}$ compared to bare Pt(544) (but still smaller than Pt(111)) and an increased $C_H$ with increasing $\theta^{step}_{Au*}$. Therefore, from the capacitance measurements shown in Figure 1 and the PZ plot analysis in Figure 2, it can be concluded that Au* truly passivates the step sites, quenching





https://doi.org/10.1021/jacs.6c07209
J. Am. Chem. Soc. 2026, 148, 31171−31180

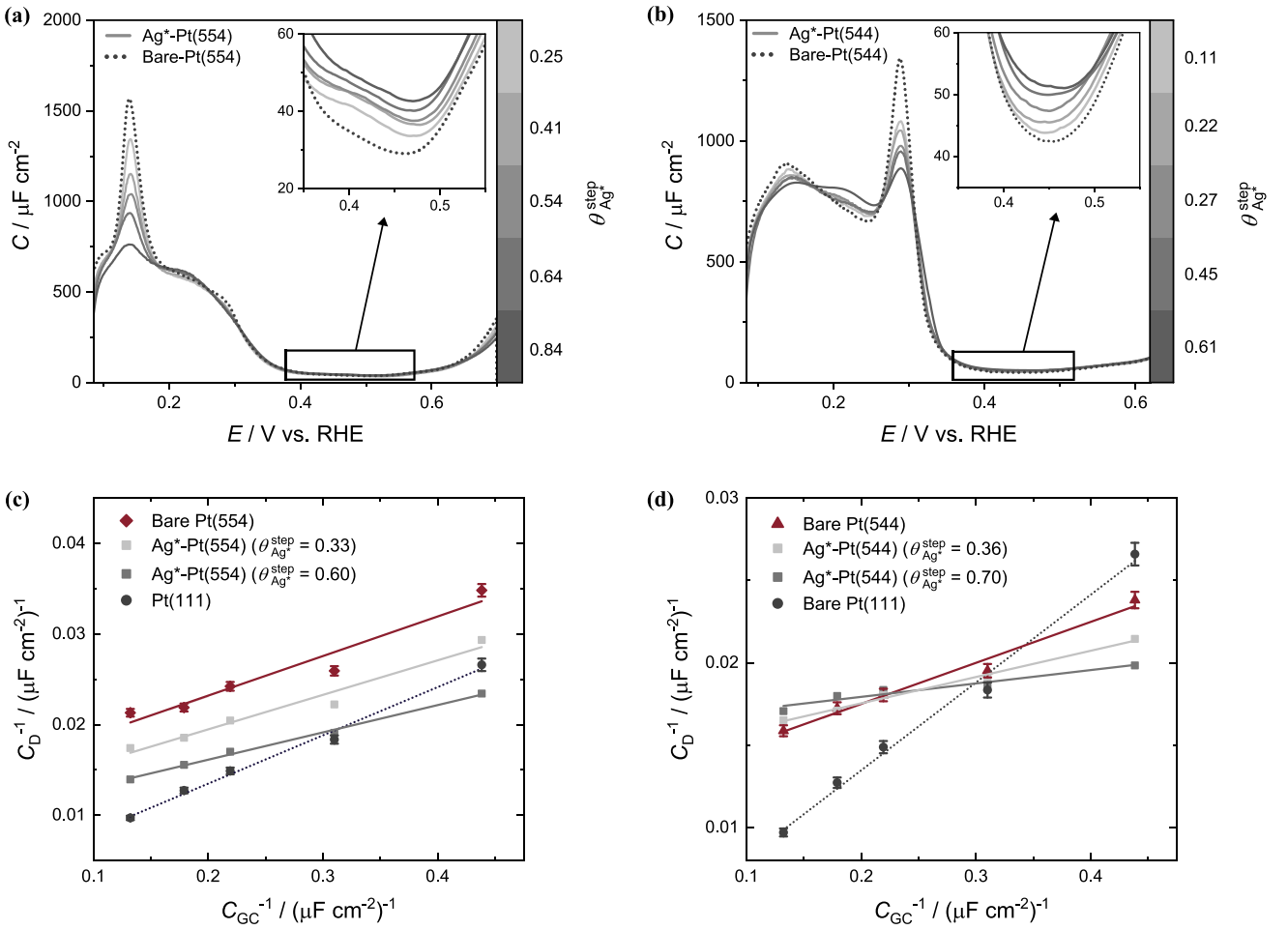


**Figure 3.** Capacitance curves for (a) Ag*$_{step}$-Pt(554) ($\theta^{step}_{Ag*}$ = 0.25−0.84), (b) Ag*$_{step}$-Pt(544) ($\theta^{step}_{Ag*}$ = 0.11 − 0.61) measured in 0.1 mM $HClO_4$ using CV, $\nu$ = 5 mV $s^{-1}$. Coverage on step ($\theta^{step}_{Ag*}$) was calculated as according to eq 2 in the Experimental Section. Corresponding CVs of the respective bare surfaces are also shown (dashed lines). Insets show zoom in of capacitance in double-layer window. Parsons−Zobel plots of (c) bare Pt(554) (brown diamonds), Ag*$_{step}$-Pt(554) ($\theta^{step}_{Ag*}$ = 0.33, 0.60) (light and dark silver squares, respectively), bare Pt(111) (black circles) and (d) bare Pt(544) (brown triangles), Ag*$_{step}$-Pt(544) ($\theta^{step}_{Ag*}$ = 0.36, 0.70) (light and dark silver squares, respectively), bare Pt(111) (black circles) measured in 0.1 mM $HClO_4$ + $x$ mM $NaClO_4$ using CV, $\nu$ = 5 mV $s^{-1}$. The Parsons−Zobel plot data for the bare surfaces are presented as mean values ± standard deviation of 3 data sets represented as error bars. Error bars are not included for the Ag*$_{step}$-modified electrodes because independently prepared adatom-modified surfaces exhibit small unavoidable variations in coverage and therefore replicate measurements primarily reflect coverage variability rather than intrinsic capacitance uncertainty.

the Pt step chemistry that inherently occurs specifically in terms of blocking the $H_{ads}/OH_{ads}$ exchange and thereby reducing the step nature-dependent trends observed for bare stepped Pt electrodes. These results also suggest that Au*$_{step}$-modification, in broader terms, provides a methodology to precisely probe the structure of the electrode/electrolyte interface by quenching the chemistry intrinsic to the Pt step sites.

It is of interest to determine whether another commonly used metal in double-layer studies due to its chemical inertness, namely Ag*,[24] would lead to a similar passivating effect as Au*. The CVs of Pt(554) and Pt(544) upon Ag*$_{step}$-modification are shown in Figures 3a and b, respectively. Similarly to Au*$_{step}$-modification, Ag*$_{step}$-modification only quenches the charge under the (110)- and (100)-step related exchange peaks but does not perturb hydrogen adsorption on the (111)-terrace sites,[21] indicating predominantly selective step site deposition. Such selective step site deposition was previously elucidated in several previous publications using primarily STM,[48,49] as well as electrochemical studies.[21,22,50]

We confirm this predominantly selective deposition by comparing the relative $\theta^{step}_{Ag*}$ calculated from the change in the charge under the step-related peak from CV (see Methods section, eq 2) for a low and high $\theta^{step}_{Ag*}$ Pt(554) surface (SI Figure 1a) to that obtained using XPS (SI Figure 1b/c) using a similar methodology to that outlined in ref 20. From this analysis, it was estimated that the $\theta^{step}_{Ag*}$(low) = 0.57 and $\theta^{step}_{Ag*}$(high) = 0.92 from CV (SI Figure 1a). The same Ag*$_{step}$/Pt(554) surfaces were then measured using XPS, from which it was estimated that the $\theta^{step}_{Ag*}$(low) = 0.56 and $\theta^{step}_{Ag*}$(high) = 0.93 (see Methods section eq 3 for details of the calculation, SI Figure 1b/c). The close agreement between the relative $\theta^{step}_{Ag*}$ values obtained by CV and XPS indicates that the Ag* indeed deposits selectively in the step sites (as was found for Au*$_{step}$/Pt($hkl$) heterobimetallic surfaces using a similar methodology[20]) and confirms the validity of using a charge-analysis to estimate the coverage from CV (eq 2, Methods section). It should be noted, however, that the reported $\theta^{step}_{Ag*}$ values from both CV and XPS should be regarded as approximate only, as uncertainties arising in the case of CV from voltammetric peak




https://doi.org/10.1021/jacs.6c07209
J. Am. Chem. Soc. 2026, 148, 31171−31180

integration introduce a limited uncertainty in the absolute coverage determination. For XPS, uncertainties related to the parameters used to calculate the $\theta^{step}_{Ag*}$ (see Table 1, Methods), as well as signal-to-noise ratio, can lead to an error in the final quantitative value obtained for the $\theta^{step}_{Ag*}$ values. These errors are difficult to quantify for both CV and XPS. Therefore, although the $\theta^{step}_{Ag*}$ values reveal a close quantitative agreement, the errors above may lead to some deviations. Importantly, however, irrespective of these uncertainties in determining the absolute Ag* coverage to a very high degree of accuracy using either technique, the systematic trends with increasing Ag* deposition are highly reproducible (*vide infra*).

Interestingly, the capacitance behavior in the double-layer window upon increasing $\theta^{step}_{Ag*}$ (Figure 3a/b) differs markedly from the behavior observed for Au*$_{step}$-modification (Figure 1). For both Pt(554) and Pt(544), Ag*$_{step}$-modification always leads to an increase in the capacitance in the double-layer window, where the increase in capacitance (ca. 20 $\mu$F cm$^{-2}$) is much larger than that observed for the changes between the capacitance values for the bare stepped Pt surfaces (e.g., Pt(544) has a capacitance of only ca. 5 $\mu$F cm$^{-2}$ greater than that of Pt(111)).[16] In fact, Ag*$_{step}$-modification leads to the same increase in the capacitance in the double-layer window independent of step nature (between (110)- and (100)-steps) and step density (SI Figures 2−4). These results suggest that Ag* itself introduces an additional capacitance contribution which dominates the capacitance response in the double-layer window over that of the intrinsic chemistry associated with the step sites for bare stepped Pt electrodes. This additional adsorption capacitance contribution introduced by the Ag* is further corroborated by the PZ plot slope behavior (Figure 3c/d), where Ag*$_{step}$-modification always leads to a lower PZ plot slope for both Pt(554) and Pt(544), decreasing more with increasing $\theta^{step}_{Ag*}$. Similar observations could be made for all other step densities (SI Figure 5). This suppressed PZ plot slope, similar to that observed for increasing (100)-step density for bare stepped Pt surfaces, is indicative of an adsorption capacitance occurring in parallel with the free-charge capacitance contributions, making it clear that Ag* is not as chemically inert as initially thought.

It should be noted that the above interpretation of the capacitance trends assumes that Au* and Ag* adatoms deposit preferentially at the Pt step sites and that their primary effect is to suppress the adsorption processes associated with these step sites (i.e., $H_{ads}/OH_{ads}$ exchange). Under this assumption, the observed capacitance changes can be interpreted predominantly in terms of site-specific passivation rather than long-range electronic perturbations of the Pt surface. Selective deposition of Au* and Ag* at Pt step sites is well-established in the literature and is supported by several observations in the present work.[20,21,23] In particular, adatom deposition selectively suppresses the step-related exchange peak while leaving the hydrogen adsorption features associated with the (111) terraces largely unaffected. In addition, the close correlation between the electrochemically estimated adatom coverages and the XPS measurements further supports preferential step-site deposition. Previous studies have also shown that Au* deposited as a single atomic row at Pt step sites does not induce significant strain in neighboring Pt atoms,[23] suggesting that long-range electronic perturbations are relatively limited in this context. To further assess the possible contribution of terrace-site modification and electronic effects, we compared the capacitance response of step-selectively modified Ag*-Pt(554) surfaces with that of an intentionally "over-deposited" Ag*-Pt(554) surface, where Ag* was deposited on both the (110)-steps and (111)-terrace sites (SI Figure 6). In contrast to the enhanced capacitance observed for step-selective Ag* deposition, the "over-deposited" Ag*-Pt(554) surface exhibits a substantially lower capacitance response, significantly smaller than that of Pt(111). This marked difference indicates that the capacitance trends reported here are dominated by the modification and passivation of adsorption processes localized at Pt step sites, rather than by a delocalized electronic perturbation extending across the (111)-terraces. Therefore, the larger capacitance observed for Ag*$_{modified}$-stepped Pt electrodes (Figure 3) can be considered to truly arise from an additional capacitance related to pseudocapacitive processes occurring on the Ag* sites deposited at the steps.

What, then, is the origin of this adsorption capacitance on Ag*? To answer this question, we must first consider what could adsorb on Ag*. As is well-established in the literature, hydrogen only binds weakly to Ag, which is, in part, related to its nearly filled *d*-band as well as the fact that its *d*-band center lies too far below the Fermi level. These factors reduce the availability of the *d*-states of Ag to strongly hybridize with adsorbates although other factors, such as the metal-bond length can also influence whether adsorption is favorable or not.[51] However, for strongly electronegative adsorbates such as hydroxyl species which could also adsorb on Ag* in this context, the usual linear correlation with the *d*-center breaks down because the polarity of the hydroxyl species leads to interactions with the Ag metal that go beyond pure electrostatics, e.g., due to donation from the oxygen lone pairs.[52,53] In fact, previous density functional theory (DFT) calculations revealed a very close agreement in the hydroxyl adsorption binding free energies for Ag* and Pt* at 0 V (where Pt* can be considered equivalent to (110)-/(100)-step sites in the context of the stepped Pt electrodes used here).[21] This suggests that Ag* has a similar affinity for hydroxyl adsorption as the step sites on bare Pt electrodes and therefore that hydroxyl species could be adsorbing here on Ag*. Besides hydroxyl adsorbates, perchlorate anions from the electrolyte may also bind to Ag. Previous work by Markovic et al. suggested that perchlorate anion adsorption may be likely as the blank voltammetry of Ag(111) in 0.1 M $HClO_4$ displays a weak signal at ca. −0.1 V (at significantly more negative potentials to the potential region of interest considered here) which they attributed to (likely) perchlorate/chloride anion adsorption. Therefore, this has the consequence that the Ag(111) surface can be considered to be covered in perchlorate/chloride anions throughout the entire potential window between hydrogen evolution and metal dissolution (and, by extension, the potential region of interest studied in this work).[35] To determine whether such perchlorate anions indeed adsorb on the Ag*$_{step}$-modified electrodes studied here, the same PZ plot analysis was carried out when adding a more specifically adsorbing anion, methanesulfonate (SI Figure 6). While the PZ plot follows a linear trend for an electrolyte containing perchlorate anions (Figure 3c/d, SI Figure 6), in the presence of the more specifically adsorbing methanesulfonate anion, the PZ plot becomes clearly nonlinear (SI Figure 6). The markedly different PZ plot trend on addition of a known specifically adsorbing anion strongly indicates that it is unlikely that perchlorate anions specifically adsorb (or least not to a significant extent). Therefore, these results corroborate our tentative hypothesis that hydroxyl species are the most





https://doi.org/10.1021/jacs.6c07209
J. Am. Chem. Soc. 2026, 148, 31171−31180

likely species to be adsorbed on the Ag* sites of Ag*$_{step}$-modified stepped Pt electrodes studied here between 0.4 and 0.6 V and are at the origin of the additional capacitance observed (Figure 3).

To concretely elucidate the possibility of OH adsorption on Ag*, we studied the CO electrooxidation reaction (COOR), which is very sensitive to the presence of such oxophilic species. On Pt electrodes, the COOR proceeds via the Langmuir−Hinshelwood mechanism (i.e., CO is oxidized via the reaction of adsorbed CO and an adsorbed oxophilic species).[27] On stepped Pt electrodes, the COOR is therefore promoted by a bifunctional effect: The presence of oxophilic species ($OH_{ads}$) at the step sites at lower potentials promotes the COOR by acting as oxygen-donating centers to which the CO adsorbed on the terraces can rapidly diffuse and react with. It follows that the COOR activity for bare stepped Pt electrodes is significantly enhanced compared to Pt(111), where the activity increases with increasing step density in accordance with an increasing proportion of oxophilic sites. This can indeed be observed in Figure 4 where both bare Pt(554) and Pt(544) display significantly enhanced COOR activities as compared to Pt(111).

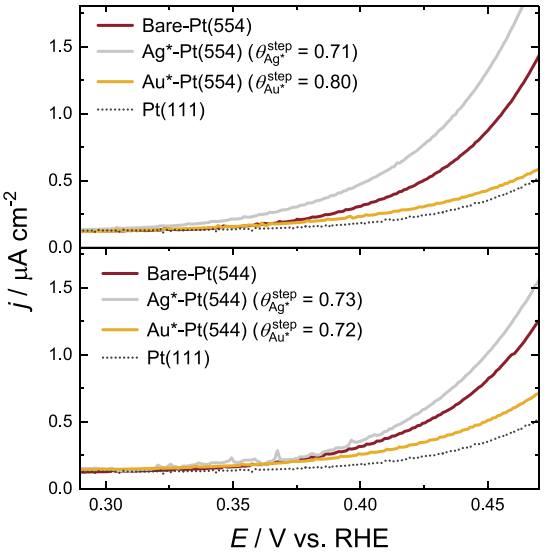


**Figure 4.** Linear sweep voltammogrms (LSVs) of CO oxidation in CO bulk-saturated 0.1 mM $HClO_4$ electrolyte for (top) bare Pt(554) (brown), Ag*$_{step}$-Pt(554) ($\theta_{Ag^*}^{step}$ = 0.71) (silver), Au*$_{step}$-Pt(554) ($\theta_{Au^*}^{step}$ = 0.80) (gold), bare Pt(111) (black dashed) and (bottom) bare Pt(544) (brown), Ag*$_{step}$-Pt(544) ($\theta_{Ag^*}^{step}$ = 0.73) (silver), Au*$_{step}$-Pt(544) ($\theta_{Au^*}^{step}$ = 0.72) (gold), bare Pt(111) (black dashed), measured in 0.1 mM $HClO_4$, $\nu$ = 10 mV s$^{-1}$.

This promotion of the COOR was also observed previously for Ru*-modified stepped Pt electrodes[29] where, in a similar way to the Au*$_{step}$/Pt($hkl$) and Ag*$_{step}$/Pt($hkl$) heterobimetallic surfaces investigated in this work, the Ru* is selectively deposited on the step sites. Ru* is known to bind oxophilic species much more strongly than Pt step sites (and Ag*), with a significantly more negative hydroxyl binding free energy.[21] As a result of this increased oxophilicity, the COOR activity of Ru*-modified stepped Pt electrodes is significantly enhanced compared to bare stepped Pt electrodes. Given that both bare Pt step sites and Ag* have similar hydroxyl binding free energies,[21] the Ag*$_{step}$/Pt($hkl$) heterobimetallic surfaces should have similar COOR activities to that of their bare counterparts. Interestingly, however, Ag*$_{step}$-Pt(554) and Ag*$_{step}$-Pt(544) both display enhanced COOR activities compared to bare Pt(554) and Pt(544), respectively (Figure 4). Note that these differences in COOR activity cannot be explained by changes in $\theta_{Ag^*}^{step}$ because XPS analysis of the Ag*$_{step}$-Pt(554) surface shows that the $\theta_{Ag^*}^{step}$ remains the same before and after CO adsorption (SI Figure 8). Instead, the promotion of the COOR upon Ag*$_{step}$-modification suggests either that the OH coverage on Ag* is higher than on bare Pt step sites, the Ag*-adsorbed OH species are more reactive toward CO oxidation than Pt−OH, or there is a different oxophilic species such as O which adsorbs on Ag* and acts to promote the COOR. Although the exact origin of the adsorption capacitance on Ag*$_{step}$/Pt($hkl$) heterobimetallic surfaces is difficult to elucidate, it is clear from the enhanced COOR activity displayed by the Ag*$_{step}$/Pt($hkl$) heterobimetallic surfaces compared to their bare counterparts that an oxygen-containing species such as OH or O adsorbs on the Ag*. The additional chemistry resulting from the adsorption of this oxygen-containing species at the Ag* sites is therefore likely the reason for the large capacitance increase observed when increasing $\theta_{Ag^*}^{step}$ (Figure 3), precluding true step passivation in this context. On the basis of this, one might be tempted to deconvolute the pseudocapacitance arising from Ag* from those of the bare stepped Pt electrodes (as the latter values are well-characterized in ref[16]). However, because the origin of the measured pseudocapacitance for Ag*$_{step}$-modified electrodes is not entirely clear, a quantitative separation of the individual contributions of the pseudocapacitance of Ag* and those originating from bare stepped Pt electrodes from voltammetric data alone is nontrivial and we do not carry out such an analysis.

In contrast to Ag*, Au*$_{step}$-modification leads to a significant inhibition of the COOR activity as compared to the bare Pt(554) and Pt(544) surfaces and their Ag*$_{step}$-modified counterparts, respectively, where the COOR activities of the Au*$_{step}$-modified surfaces tend toward that of Pt(111) (Figure 4). The COOR activity of Pt(554) was similarly found previously to become inhibited upon Bi* and Te*-modification and ascribed to a decrease in the amount of oxophilic species present at the step sites after modification relative to the bare surface due to blocking of the intrinsic step-site chemistry.[47] Therefore, the inhibited COOR activity of the Au*$_{step}$-modified surfaces taken together with both the capacitance and PZ plot behavior (Figure 1/2) corroborates that Au* is truly chemically inert in this context and does not adsorb any oxophilic species, i.e., true step passivation can be achieved for Au*$_{step}$/Pt($hkl$) heterobimetallic surfaces where this was not achievable for Ag*$_{step}$/Pt($hkl$) heterobimetallic surfaces. It also follows from these COOR activity results that by changing the oxophilicity of the metal adatom deposited at the step site, the corresponding COOR activity can be tuned, serving as a reminder of the precision with which electrocatalytic activity can be controlled in this context.

## CONCLUSION

In this work, we have shown that selective Au* electrodeposition results in successful passivation of the step sites of stepped Pt single crystal surfaces. As a result, the step-nature dependent trends observed on bare stepped Pt single crystals, namely, a decreasing capacitance in the double-layer window with increasing (110)-step density, but an increasing capacitance with increasing (100)-step density, could be




https://doi.org/10.1021/jacs.6c07209
J. Am. Chem. Soc. 2026, 148, 31171−31180

selectively reversed upon Au*$_{step}$-modification by selectively blocking the $H_{ads}/OH_{ads}$ exchange process intrinsic to (110)-/(100)-step sites on bare stepped Pt, highlighting the role of adsorption at step sites on the capacitive behavior of these stepped Pt electrodes. This reversal of the step-dependent trends observed for bare stepped Pt electrodes was further proven by a Parsons−Zobel plot analysis, where the slope was found to increase upon Au*$_{step}$-modification for only the (100)-stepped surfaces, but no change in slope was observed for (110)-stepped surfaces.

Interestingly, when using another commonly used metal employed for double-layer studies—Ag*—we found that the capacitance response in the double-layer window became convoluted by a large (adsorption) capacitance introduced by the Ag* itself. Owing to an enhanced CO oxidation activity of the Ag*$_{step}$-modified electrodes with respect to their Au*$_{step}$-modified and bare counterparts, we attribute this increased capacitance to the presence of oxophilic species adsorbing on the Ag* in a potential-dependent manner. Au*$_{step}$-modification, on the other hand, was found to significantly inhibit the CO oxidation reaction. Therefore, true step passivation was only achieved through Au*$_{step}$-modification, whereas Ag*$_{step}$-modification led to additional chemical effects. This work therefore provides a new methodology to probe the structure of the electrical double-layer at a fundamental level by disentangling the adsorption and geometric contributions to the interfacial capacitance at more structurally complex Pt/electrolyte interfaces, thereby highlighting the marked influence of adsorption at step sites on the capacitive behavior of Pt. On top of tuning the electrical double-layer structure, we show here that adatom modification can also tune the electrocatalytic activity of stepped Pt single crystals for CO oxidation to a remarkably precise degree by varying the oxophilicity of the adatom chosen.

## ■ ASSOCIATED CONTENT

### Data Availability Statement

Data will be made available on request.

### Supporting Information

The Supporting Information is available free of charge at https://pubs.acs.org/doi/10.1021/jacs.6c07209.

> The supporting experimental evidence for determining the Ag* coverage from CV and XPS, capacitance curves for (110)- and (100)-stepped Pt electrodes with different step densities as a function of Ag* coverage, Parsons−Zobel plots for Ag*$_{step}$-modified (110)- and (100)-stepped Pt electrodes with different step densities compared to their bare counterparts, capacitance curves for an "over-deposited" Ag*-modified Pt(554) surface, Parsons−Zobel plots for bare and Ag*$_{step}$-Pt(554) in the presence of a nonspecifically and weakly adsorbing anion, and the change in Ag* coverage on Pt(554) before and after CO adsorption from XPS (PDF)

## ■ AUTHOR INFORMATION


### Corresponding Author

**Marc T. M. Koper** − *Leiden Institute of Chemistry, Leiden University, 2333 CC Leiden, The Netherlands;* orcid.org/0000-0001-6777-4594; Email: m.koper@lic.leidenuniv.nl

### Authors

**Nicci L. Fröhlich** − *Leiden Institute of Chemistry, Leiden University, 2333 CC Leiden, The Netherlands;* orcid.org/0009-0004-4655-6415

**Yifan Hu** − *Leiden Institute of Chemistry, Leiden University, 2333 CC Leiden, The Netherlands*

**Alfred Larsson** − *Leiden Institute of Chemistry, Leiden University, 2333 CC Leiden, The Netherlands*

Complete contact information is available at: https://pubs.acs.org/10.1021/jacs.6c07209


### Notes

The authors declare no competing financial interest.

## ■ ACKNOWLEDGMENTS

NLF and MTMK received funding from the European Research Council (ERC) (Advanced Grant No. 101019998 "FRUMKIN"). AL acknowledges financial support from the Swedish Research Council (2024-00351).

## ■ REFERENCES


(1) Bard, A. J.; Faulkner, L. R. *Electrochemical Methods Fundamentals and Applications* (John Wiley & Sons, Inc., 2001).

(2) Koper, M. T. M. Blank voltammetry of hexagonal surfaces of Pt-group metal electrodes: Comparison to density functional theory calculations and ultra-high vacuum experiments on water dissociation. *Electrochim. Acta* **2011**, *56*, 10645−10651.

(3) Rizo, R.; Herrero, E.; Climent, V.; Feliu, J. M. On the nature of adsorbed species on Platinum Single Crystal electrodes. *Curr. Opin. Electrochem.* **2023**, *38*, 101240.

(4) Pajkossy, T.; Kolb, D. M. Double layer capacitance of Pt(111) single crystal electrodes. *Electrochim. Acta* **2001**, *46*, 3063−3071.

(5) Fröhlich, N. L.; Eggebeen, J. J. J.; Koper, M. T. M. Measurement of the double-layer capacitance of Pt(111) in acidic conditions near the potential of zero charge. *Electrochim. Acta* **2024**, *494*, 144456.

(6) Ojha, K.; Arulmozhi, N.; Aranzales, D.; Koper, M. T. M. Double Layer at the Pt(111)-Aqueous Electrolyte Interface: Potential of Zero Charge and Anomalous Gouy-Chapman Screening. *Angew. Chem., Int. Ed.* **2020**, *59*, 711−715.

(7) Ojha, K.; Doblhoff-Dier, K.; Koper, M. T. M. Double-layer structure of the Pt(111)-aqueous electrolyte interface. *Proc. Natl. Acad. Sci. U. S. A.* **2022**, *119*, No. e2116016119.

(8) Doblhoff-Dier, K.; Koper, M. T. M. Electric double layer of Pt(111): Known unknowns and unknown knowns. *Curr. Opin. Electrochem.* **2023**, *39*, 101258.

(9) Doblhoff-Dier, K.; Koper, M. T. M. Modeling the Gouy-Chapman Diffuse Capacitance with Attractive Ion-Surface Interaction. *J. Phys. Chem. C* **2021**, *125*, 16664−16673.

(10) Fröhlich, N. L.; Sjö, H.; Mascaró, F. V.; Koper, M. T. M. Correlating surface structure and electrochemical properties of polycrystalline platinum electrodes. *Electrochim. Acta* **2026**, *548*, 147977.

(11) Rizo, R.; et al. Analysis of the OH Coverage on Low-Coordinated Pt Sites at Low Potentials. *ACS Electrochemistry* **2025**, *1*, 351−359.

(12) Rizo, R.; et al. Investigating the presence of adsorbed species on Pt steps at low potentials. *Nat. Commun.* **2022**, *13*, 2550.

(13) Koper, M. T. M. Structure sensitivity and nanoscale effects in electrocatalysis. *Nanoscale* **2011**, *3*, 2054−2073.

(14) Feliu, J. M.; Herrero, E. Pt single crystal surfaces in electrochemistry and electrocatalysis. *EES Catalysis* **2024**, *2*, 399−410.

(15) Xue, S.; et al. Impact of Pt(*hkl*) Electrode Surface Structure on the Electrical Double Layer Capacitance. *J. Am. Chem. Soc.* **2024**, *146*, 3883−3889.

(16) Fröhlich, N. L.; et al. A comprehensive model for the electric double layer of stepped platinum electrodes. *Nat. Chem.* **2026**, *18*, 905−912.
(17) Tanaka, H.; et al. Infrared Reflection Absorption Spectroscopy of OH Adsorption on the Low Index Planes of Pt. *Electrocatalysis* **2015**, *6*, 295−299.
(18) Chen, X.; McCrum, I. T.; Schwarz, K. A.; Janik, M. J.; Koper, M. T. M. Co-adsorption of Cations as the Cause of the Apparent pH Dependence of Hydrogen Adsorption on a Stepped Platinum Single-Crystal Electrode. *Angew. Chem., Int. Ed.* **2017**, *56*, 15025−15029.
(19) McCrum, I. T.; Chen, X.; Schwarz, K. A.; Janik, M. J.; Koper, M. T. M. Effect of Step Density and Orientation on the Apparent pH Dependence of Hydrogen and Hydroxide Adsorption on Stepped Platinum Surfaces. *J. Phys. Chem. C* **2018**, *122*, 16756−16764.
(20) Kodama, K.; Jinnouchi, R.; Takahashi, N.; Murata, H.; Morimoto, Y. Activities and Stabilities of Au-Modified Stepped-Pt Single-Crystal Electrodes as Model Cathode Catalysts in Polymer Electrolyte Fuel Cells. *J. Am. Chem. Soc.* **2016**, *138*, 4194−4200.
(21) McCrum, I. T.; Koper, M. T. M. The role of adsorbed hydroxide in hydrogen evolution reaction kinetics on modified platinum. *Nat. Energy* **2020**, *5*, 891−899.
(22) Goyal, A.; Louisia, S.; Moerland, P.; Koper, M. T. M. Cooperative Effect of Cations and Catalyst Structure in Tuning Alkaline Hydrogen Evolution on Pt Electrodes. *J. Am. Chem. Soc.* **2024**, *146*, 7305−7312.
(23) Liu, G.; et al. Site-specific reactivity of stepped Pt surfaces driven by stress release. *Nature* **2024**, *626*, 1005−1010.
(24) Valette, G. Double layer on silver single crystal electrodes in contact with electrolytes having anions which are slightly specifically adsorbed: Part III. The (111) face. *J. Electroanal. Chem. Interfacial Electrochem.* **1989**, *269*, 191−203.
(25) Hamelin, A.; Vitanov, T.; Sevastyanov, E.; Popov, A. The electrochemical double layer on sp metal single crystals: The current status of data. *J. Electroanal. Chem. Interfacial Electrochem.* **1983**, *145*, 225−264.
(26) Samjeske, G.; Xiao; Baltruschat, H. Ru Decoration of Stepped Pt Single Crystals and the Role of the Terrace Width on the Electrocatalytic CO Oxidation. *Langmuir* **2002**, *18*, 4659−4666.
(27) Lebedeva, N. P.; Koper, M. T. M.; Herrero, E.; Feliu, J. M.; van Santen, R. A. Cooxidation on stepped Pt[n(111)×(111)] electrodes. *J. Electroanal. Chem.* **2000**, *487*, 37−44.
(28) Koper, M. T. M.; Lebedeva, N. P.; Hermse, C. G. M. Dynamics of CO at the solid/liquid interface studied by modeling and simulation of CO electro-oxidation on Pt and PtRu electrodes. *Faraday Discuss.* **2002**, *121*, 301−311.
(29) Massong, H.; Wang, H.; Samjeské, G.; Baltruschat, H. The co-catalytic effect of Sn, Ru and Mo decorating steps of Pt(111) vicinal electrode surfaces on the oxidation of CO. *Electrochim. Acta* **2001**, *46*, 701−707.
(30) Fröhlich, N.; et al. Effect of trace impurities in perchloric acid on blank voltammetry of Pt(111). *Electrochim. Acta* **2023**, *466*, 143035.
(31) Clavilier, J.; Faure, R.; Guinet, G.; Durand, R. Preparation of monocrystalline Pt microelectrodes and electrochemical study of the plane surfaces cut in the direction of the {111} and {110} planes. *J. Electroanal. Chem. Interfacial Electrochem.* **1980**, *107*, 205−209.
(32) Clavilier, J. The role of anion on the electrochemical behaviour of a {111} platinum surface; an unusual splitting of the voltammogram in the hydrogen region. *J. Electroanal. Chem. Interfacial Electrochem.* **1980**, *107*, 211−216.
(33) O'Keeke, T. J. Pourbaix Diagrams. In *Encyclopedia of Materials: Science and Technology*; Buschow, K. H. J., et al., Eds.; pp 7774−7781 (Elsevier, Oxford, 2001).
(34) McCafferty, E. *Introduction to Corrosion Science* (Springer Science & Business Media, 2009).
(35) Blizanac, B. B.; Ross, P. N.; Markovic, N. M. Oxygen electroreduction on Ag(111): The pH effect. *Electrochim. Acta* **2007**, *52*, 2264−2271.
(36) Javed, H.; et al. A laboratory-based electrochemical NAP-XPS system for operando electrocatalysis studies. *Vacuum* **2025**, *231*, 113755.
(37) Larsson, A.; et al. Thickness and composition of native oxides and near-surface regions of Ni superalloys. *J. Alloys Compd.* **2022**, *895*, 162657.
(38) Yeh, J. J.; Lindau, I. Atomic subshell photoionization cross sections and asymmetry parameters: $1 \leqslant Z \leqslant 103$. *At. Data Nucl. Data Tables* **1985**, *32*, 1−155.
(39) Parry, D. E. Atomic calculation of photoionization cross-sections and asymmetry parameters. *Rapid Commun. Mass Spectrom.* **1994**, *8*, 579.
(40) Climent, V.; Feliu, J. M. Surface Electrochemistry with Pt Single-Crystal Electrodes. *Advances in Electrochemical Science and Engineering* **2017**, *17*, 1−57.
(41) Valls Mascaró, F.; Koper, M. T. M.; Rost, M. J. Step bunching instability and its effects in electrocatalysis on platinum surfaces. *Nat. Catal.* **2024**, *7*, 1165−1172.
(42) Klein, J.; et al. Selective Modification and Probing of the Electrocatalytic Activity of Step Sites. *J. Am. Chem. Soc.* **2020**, *142*, 1278−1286.
(43) Jinnouchi, R.; Suzuki, K. K. T.; Morimoto, Y. DFT calculations on electro-oxidations and dissolutions of Pt and Pt-Au nanoparticles. *Catal. Today* **2016**, *262*, 100−109.
(44) Deng, L.; Hu, W.; Deng, H.; Xiao, S. Surface Segregation and Structural Features of Bimetallic Au-Pt Nanoparticles. *J. Phys. Chem. C* **2010**, *114*, 11026−11032.
(45) Yamakawa, S.; Asahi, R.; Koyama, T. Surface segregations in platinum-based alloy nanoparticles. *Surf. Sci.* **2014**, *622*, 65−70.
(46) Björling, A.; Ahlberg, E.; Feliu, J. M. Kinetics of surface modification induced by submonolayer electrochemical oxygen adsorption on Pt(1 1 1). *Electrochem. commun.* **2010**, *12*, 359−361.
(47) Chen, Q.-S.; Berna, A.; Climent, V.; Sun, S.-G.; Feliu, J. M. Specific reactivity of step sites towards CO adsorption and oxidation on platinum single crystals vicinal to Pt(111). *Phys. Chem. Chem. Phys.* **2010**, *12*, 11407−11416.
(48) Domke, K. F.; Xiao, X.-Y.; Baltruschat, H. The formation of two Ag UPD layers on stepped Pt single crystal electrodes and their restructuring by co-adsorption of CO. *Electrochim. Acta* **2009**, *54*, 4829−4836.
(49) Gambardella, P.; Blanc, M.; Brune, H.; Kuhnke, K.; Kern, K. One-dimensional metal chains on Pt vicinal surfaces. *Phys. Rev. B* **2000**, *61*, 2254−2262.
(50) Xu, J.; Abd-El-Latif, A.-E.-A. A.; Chen, Y.-X.; Baltruschat, H. Electrodeposition of silver on stepped platinum electrode surfaces with (100)-oriented terraces: Generation of confined reaction sites. *J. Electroanal. Chem.* **2014**, *716*, 93−100.
(51) Zheng, H.; Li, H.; Luo, L.; Zhao, Z.; Henkelman, G. Factors that influence hydrogen binding at metal-atop sites. *J. Chem. Phys.* **2021**, *155*, 024703.
(52) Karlberg, G. S. Adsorption trends for water, hydroxyl, oxygen, and hydrogen on transition-metal and platinum-skin surfaces. *Phys. Rev. B* **2006**, *74*, 153414.
(53) Xin, H.; Linic, S. Communications: Exceptions to the d-band model of chemisorption on metal surfaces: The dominant role of repulsion between adsorbate states and metal d-states. *J. Chem. Phys.* **2010**, *132*, 221101.




https://doi.org/10.1021/jacs.6c07209
J. Am. Chem. Soc. 2026, 148, 31171−31180